COVER SHEET (SIGNED BY THE PRINCIPAL INVESTIGATORS)

Federal Ministry of Education and Research (BMBF), Germany	**Ministry of Science, Technology and Space (MOST), Israel**

Joint German-Israeli Water Technology Research Program

JOINT FINAL REPORT

For the Period: June 2020 until Dec 2023 (Final report)

German Project Number 02WIL1555 Israeli Project Number 3-17010

Title of German Project: Nano-electro membrane processes for micropollutant removal in water reuse

Title of Israeli Project: Nano-electro membrane processes for micropollutant removal in water reuse

Principal Investigator(s) -- including Institution(s) and Department(s):

Prof. Daniel Mandler
The Hebrew University of Jerusalem (HUJI), Institute of Chemistry

Prof Dr. Ing Andrea Iris Schäfer
Karlsruhe Institute of Technology (KIT), Institute for Advanced Membrane Technology (IAMT)

Signatures:
Israeli Principal Investigator(s):

Daniel Mandler Daniel Mandler Date: 17.4.2024

German Principal Investigator(s):

Andrea Schaefer Andrea Schäfer Date: 15.5.2024

Abstract: The original objectives of the proposal were: i) integrate nanotechnologies with electrochemical reactions in a composite membrane, ii) allow in-situ monitoring of micropollutants (MPs) in polluted or reused (treated) water, and iii) remove micropollutants effectively in water reuse.

The project involved three groups, one headed by Prof. Schäfer from Karlsruhe Institute of Technology (KIT) whereas the two Israeli groups were one from the Technion (Tech), headed by Prof. Raphael Semiat and Prof. Daniel Mandler from the Hebrew University (HUJI).

The division of work among partners was that the group in KIT worked mostly on the photocatalytic and electrochemical degradation of steroid hormone (SH) in a membrane reactor. Moreover, they scaled up the electrochemical filtration system from 2 to 20 cm^2, followed by an evaluation and optimization of its efficacy in SH micropollutant removal. The group at the Technion focused on Fenton-like oxidation processes for removing propoxur, a micro-pollutant compound, from synthetic reverse osmosis concentrate (ROC) solution. A hierarchical methodology for determining the electro-removal mechanisms of micropollutants with different properties was developed. The group at the Hebrew University studied the electrochemical degradation of nonyl-phenol, which is also a common micropollutant using a flow-through cell based also on carbon nanotubes (CNTs). Furthermore, the group has studied the electrochemical generation of reactive oxygen species (ROS) through the oxygen reduction reaction (ORR).

In spite of the difficult times due to the COVID-19 epidemic, the collaboration continued all the time and included mutual visits of the PIs and also a long-stay visit of a student from KIT at HUJI. A few publications came out of this project, a few more are under preparation. We believe that most if not all of the objectives were accomplished and we have definitely made significant progress in the integration of photocatalytical and electrochemical methods in flow-through membrane systems that are based on different materials.

Following are the summary of the project progress and detailed descriptions of the activities of the three groups:

Table 1. The project progress compared with the plan.

Milestone in the proposal	**Timetable**	**Status**	**Comments**
M.1. Construct a flow-through filtration cell (HUJI, TECH, KIT)	01.2021 - 12.2021	Finished	- A flow-through electrochemical filtration system was constructed - A commercial electrochemical cell was purchased and was used for the investigation of the protocol for electrochemical filtration experiment - A micro-electrochemical crossflow cell with membrane area of 2 cm^2 was designed and externally constructed
M.2. Investigate electro-Fenton (EF) and electro-adsorption of the target micro-pollutants (TECH, HUJI)	03.2021 - 12.2021	Finished	- The faradaic efficiency of H_2O_2 and OH radcials was studied by the ORR using different carbonaceous materials and different catalysts.
M.3. Select target micropollutants and develop analytical methodology for micropollutant degradation at single ng/L limit of detection (HUJI, TECH, KIT)	01.2021 - 12.2021	Finished	-An ultra-high-performance liquid chromatograph coupling with a flow scintillator analyzer (UHPLC-FSA) method was developed by Roman Lyubimenko for radiolabeled steroid hormones SHs analysis [1] -A combined method integrating UHPLC-FSA and liquid scintillation counting (LSC) was developed to differentiate the concurrent electrochemical adsorption and degradation processes during micropollutant removal
M.4. Understand and optimize the purification processes and the removal of the target micropollutants (HUJI, TECH, KIT)	06.2021 - 5.2022	Finished	- The electrochemistry of micropollutants on the CNTs membrane [2, 3] was examined to understand and optimize the process - The limiting factors of the micropollutant removal were determined at varying operational conditions
M.5. Evaluate the feasibility of the NME process by comparing the electro-Fenton with Fenton oxidation (TECH)	01.2022 - 12.2022	Finished	-Comparative experiments of MP model compound (PR) removal by Fenton- and electro-Fenton-based oxidation processes were conducted aimed at studying the effects of various parameters, including reaction time, pH, molar ratio of H_2O_2 to iron, PR concentration, and reverse osmosis concentrate composition
M.6. Model the reaction dynamic and compare with	01.2022 – 12.2023	Finished	The mechanism in terms of the predominant reactive species contributing to the micropollutant degradation was examined for the

photocatalytic processes for micropollutant degradation (KIT)			electrochemical and photocatalytic membrane process
M.7. Model and improve the NEM using COMSOL Multiphysics software (TECH)	03.2022 – 06.2023	Not Finished	- Insufficient experimental data within the time frame hindered the development of a validated mode
M.8. Design, construct and test of a scaled-up NEM system (HUJI, TECH, KIT)	10.2022 – 12.2023	Finished	The scaled-up system was upscaled from 2 to 20 cm^2 A 3D printed flow cell was designed and printed.
Final analyses and reporting (HUJI, TECH, KIT)	10.2023-04.2024	Finished	Submitted

1. SCIENTIFIC OR TECHNICAL RESULTS

<u>Technion:</u>

Abstract

A publication titled "Competitive Study of Homogeneous and Heterogeneous Fenton-like Flow-through Propoxur Oxidation in ROC Solution," which acknowledges the project, has been published in Water Science & Technology Journal in 2023. This paper presents an investigation into the effectiveness of homogeneous and heterogeneous Fenton-like oxidation processes for removing propoxur, a micro-pollutant compound, from synthetic reverse osmosis concentrate (ROC) solution. Two electrolytic cell configurations were examined: divided and undivided in both the cathode is a porous fiber felt cathode (GF), where in the latter, an ion exchange membrane separates the cell into anodic and cathodic compartments. A hierarchical methodology for determining the electro-removal mechanisms of micropollutants with different properties was developed, and a manuscript is currently under preparation. In this methodology, the electrochemical removal mechanisms of micropollutant compounds in both cell configurations were determined through the systematic elimination of specific mechanisms. This approach facilitated the delineation of the individual contributions of each mechanism, including direct and indirect anodic oxidation, oxidation by electro-generated hydrogen peroxide, adsorption onto GF and/or ion exchange membrane, and electro-adsorption onto GF and/or ion exchange membrane. The impact of various conditions such as current density, catalyst dosage, and mixing rate on the removal of propoxur in the homogeneous electro-Fenton process (i.e., H_2O_2/Fe^{2+}) was investigated in both electrolytic cell configurations.

Body of report:

Published article: A publication acknowledging the project titled "Competitive Study of Homogeneous and Heterogeneous Fenton-like Flow-through Propoxur Oxidation in ROC Solution" was published in Water Science & Technology (Volume 87, Issue 11, 2023, 2890–2904). This paper presents an investigation into the efficacy of homogeneous and heterogeneous Fenton-like oxidation processes for removing propoxur (PR), a micro-pollutant compound, from a synthetic reverse osmosis concentrate (ROC) solution. A submerged ceramic membrane reactor operated in continuous mode was employed for the study. A newly synthesized amorphous heterogeneous catalyst, ferrihydrite (Fh), was characterized, revealing a layered porous structure of nanoparticles. The ceramic membrane demonstrated a rejection rate of over 99.6% for Fh, indicating its sustainability. While homogeneous catalysis (Fe^{3+}) showed superior activity in PR removal compared to Fh initially, increasing H_2O_2 and Fh concentrations at a constant molar ratio resulted in PR oxidation efficiencies equal to those catalyzed by Fe^{3+}. The ionic composition of the ROC solution hindered PR oxidation, but increased residence time improved removal efficiency up to 87% at 88 min. Overall, the study underscores the potential of heterogeneous Fenton-like processes catalyzed by Fh in continuous operation mode.

Electrolytic cell configuration: Two electrolytic cell configurations were studied: divided and undivided, both at a volume of 50 mL. Schematics of both are displayed in Figure 1. The undivided electrolytic cell is equipped with parallel electrodes, a DSA plate ($Ti/RuO_2/IrO_2$, Whizzo S&T, China) as the anode, and a porous graphite fiber felt (GF) as the cathode. The dimensions of the electrodes are 100 x 25 mm (L x W) with a thickness of 1.5 mm and a 6 mm gap between them. The electrodes are connected to a DC power supply (0–5 A, 0–30 V) that provides a constant current. The same electrode layout is used in the divided cell, where an ion exchange membrane (Nafion N-424, Ion Power Inc.) separates the cell into anodic and cathodic compartments. The electrolyte (200 mL) can circulate within the cell (batch mode) or be fed to the cell (continuous mode, indicated by dashed lines in the Figure 1) using a pump. An air blower is used for air sparging, which is distributed through a porous stone.

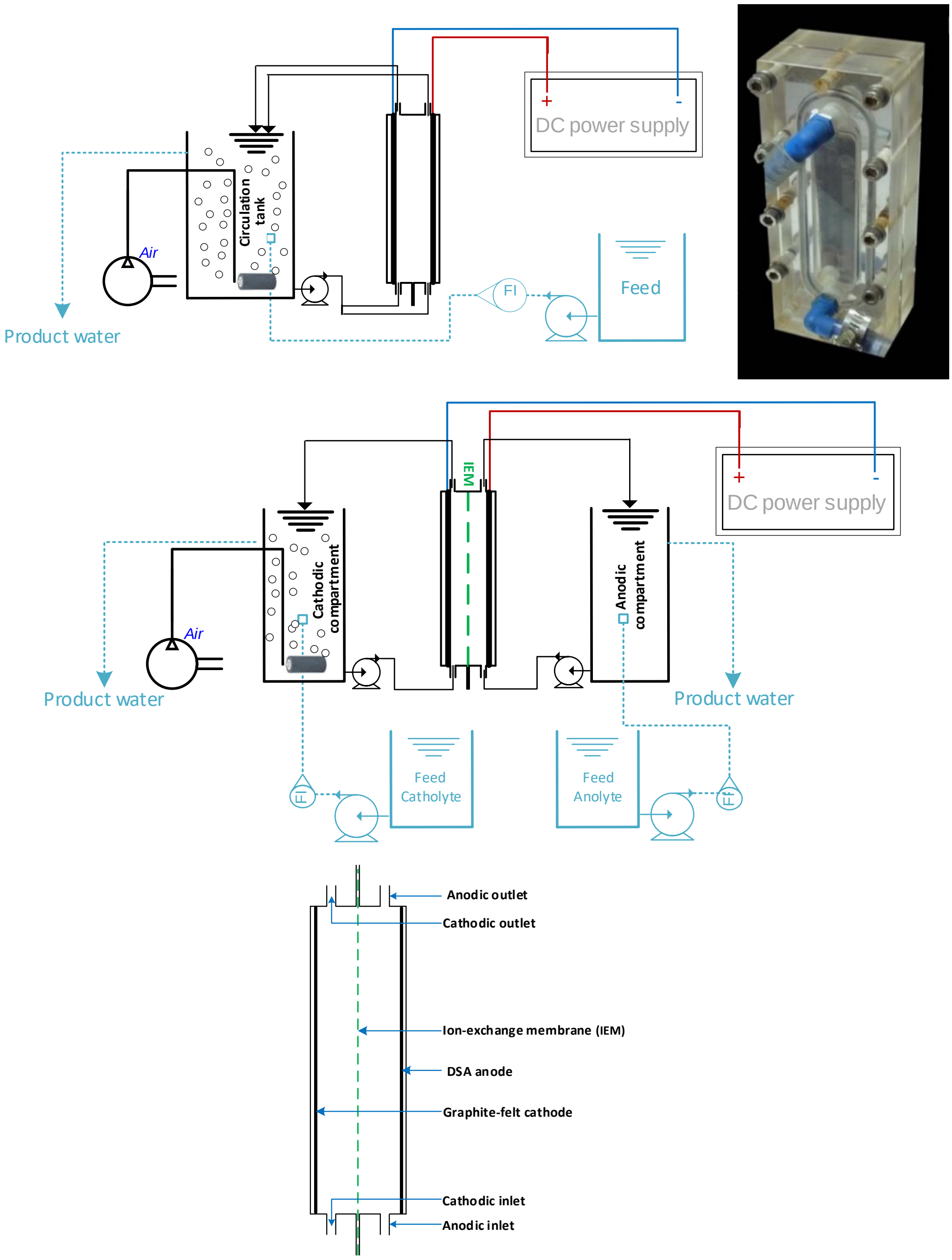

Figure 1. Schematics of the (a) undivided electrochemical systems including an image of the electrolytic cell; (b) undivided electrochemical system; (c) electrolytic cell. The difference between the divided and undivided cell is the ion exchange membrane (IEM), represented by the dashed green line

Development of a method for determining the electro-removal mechanisms of MPs:

Publication titled "Development of a Hierarchical Methodology for Determining the Mechanisms of Micropollutant Electro-removal" is being prepared. In the developed methodology, the electrochemical removal mechanisms of micropollutant (MP) compounds in both undivided and divided cells were determined through the systematic elimination of specific mechanisms. This approach enabled the delineation of the individual contributions of each mechanism, including direct and indirect anodic oxidation, oxidation by hydrogen peroxide, adsorption onto GF and/or ion exchange membrane, and electro-adsorption onto GF and/or ion exchange membrane.

For example, batch experiments revealed that there was no adsorption of PR onto the GF within 24 h when no current was applied. The observed 10.6% PR removal was attributed to the simultaneous occurrence of three mechanisms: anodic oxidation, electro-adsorption onto the GF, and anodic oxidation of the electro-generated H_2O_2. The inhibition of the anodic oxidation of H_2O_2 is achieved by preventing its generation through the addition of N_2+Na_2SO_3. The addition of KI, acting as a surface-bound hydroxyl radical scavenger, suppresses both ·OH and direct electron transfer oxidation processes, thereby inhibiting anodic oxidation. The combined addition of KI with N_2 and Na_2SO_3 suppresses both potential anodic and hydrogen peroxide reactions. In this example, by eliminating the anodic reactions, it was concluded that the predominant removal mechanism for PR was electro-adsorption onto the GF.

In the divided cell, adsorption/electro-adsorption onto the IEM may also contribute to the MPs removal mechanism. Close PR removals were obtained in the cathode and anode compartments with and without applying current (Figure 2). In the absence of applied current, 12% and 14% of PR were removed within 60 min at the anode and cathode compartments, respectively, indicating adsorption onto the IEM. At current density of 1 mA/cm^2, PR removal increased to 22% and 25% at the cathode and anode compartments, respectively. The electro-adsorption of the IEM is evaluated by subtracting the electro-adsorption of the GF and the adsorption of the IEM.

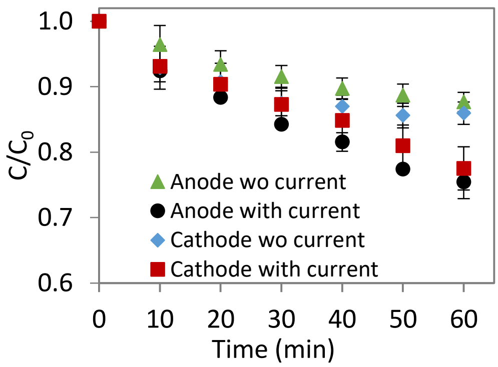

Figure 2. PR removal anode and cathode compartments without and with applied current (0.1 M Na_2SO_4, air purging, pH 3, 1.0 mA/cm^2)

In addition to the electrolytic cell configurations, the properties of the MPs affect their removal mechanism. Five pesticides, Parathion, Propoxur, Methomyl, Methamidophos, and Oxamyl- were studied, each exhibiting different properties such as the level of hydrophilicity and hydrophobicity, as shown in Figure 3a. Depending on the properties, MPs develop different types of mechanisms. For example, the compound charge is responsible for short-distance interactions with the GF and/or the ion-exchange membrane, as shown schematically in Figure 3b.

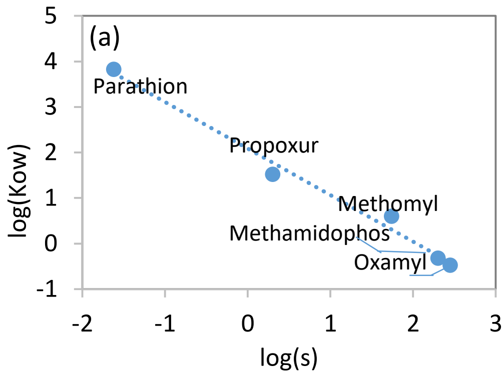

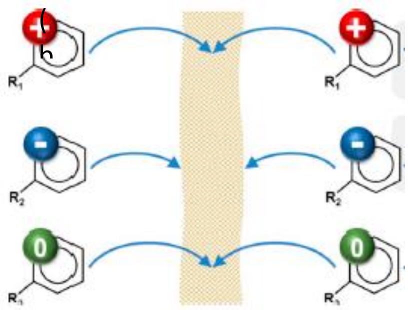

Figure 3. (a) Hydrophilicity and hydrophobicity of the tested MPs and (b) MPs adsorption onto IEM at a different compound charge

Parameter study: The homogenous electro-Fenton process (i.e., H_2O_2/Fe^{2+}) was studied at various conditions such as current density, catalyst dosage, and mixing rate for the removal of PR in both divided and undivided electrolytic cells. It should be noted that in the divided cell, emphasis was given to the cathodic compartment, where the catalytic oxidation process takes place.

In-situ production of H_2O_2 was measured in both divided and undivided cell configurations. Both electrolytic cell configurations demonstrated an increase in the H_2O_2 generation with the current density from 0.28 to 1.01 mA/cm^2 until reaching a relatively narrow plateau up to 1.40 mA/cm^2. Subsequently, a further increase in current density up to 2.13 mA/cm^2 led to a decrease in the H_2O_2 generation (Figure 4a). This may be attributed to the enhancement of H_2O_2 decomposition in the bulk solution and on the anode surface, as well as to the higher selective of 4e$^-$ ORR reaction. Electro-production of H_2O_2 in the divided cell was four times higher than that in the undivided cell probably due to anodic decomposition of the H_2O_2.

As seen in Figure 4b, PR removal increased as the current density was raised, corresponding to the enhanced electro-generation of H_2O_2 (Figure 4a). However, a subsequent increase in the current density resulted in diminished PR removal, consistent with the reduced generation of H_2O_2. PR removal in the divided cell was 1.6 times higher than that in the undivided cell. Divided electrolytic cells achieve higher reaction rates due to the elimination of side reactions that occur on the anode.

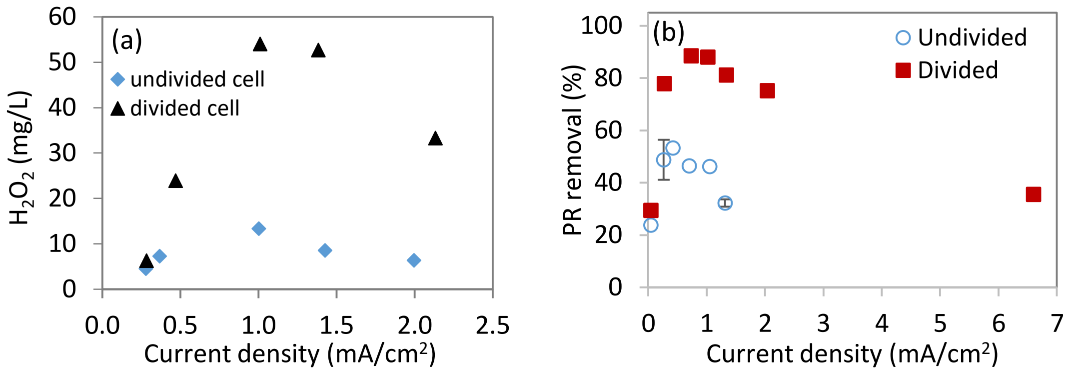

Figure 4. (a) H_2O_2 electro-generation and (b) catalytic PR removal in the divided and undivided electrolytic cells as a function of the current density (0.1 M Na_2SO_4, air purging, pH 3, 17.9 μM Fe^{2+}, 60 min reaction)

The effect of catalyst dosage was evaluated in the range from 0 to 40 μM Fe^{2+}. In both cell configurations, an increase in the Fe^{2+} concentration resulted in enhanced removal of the PR, as displayed in Figure 5. At a concentration of 40 μM Fe^{2+}, 96% of PR was removed within 40 min. The increase in Fe^{2+} concentration leads to higher concentrations of hydroxyl radicals, manifested by higher removal efficiency.

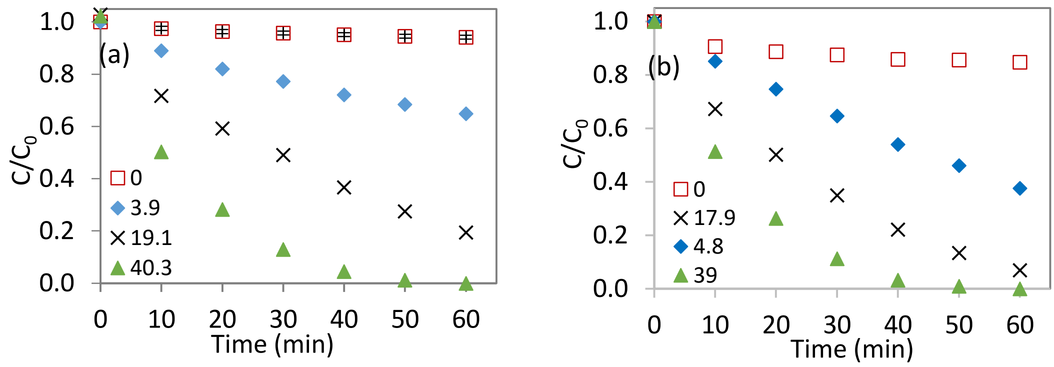

Figure 5. Catalytic removal of PR in the (a) undivided and (b) divided electrolytic cells as a function of the catalyst (Fe^{2+}) μM concentration (0.1 M Na_2SO_4, air purging, pH 3, 0.3 mA/cm^2, 60 min reaction)

As mixing can affect both the mass transfer between the MP compound and the electrodes and the current density, experiments were conducted at a constant current density of 0.3 mA/cm². The results are displayed in Figure 6. An improvement in PR removal efficiency was observed by increasing the mixing rate from 50 to 100 mL/min. Further increase to 150 mL/min resulted in a slight increase. The superior performance of the undivided cell is evident in all mixing rates.

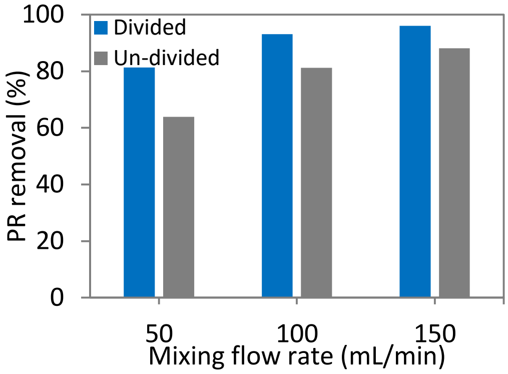

Figure 6. Catalytic removal of PR in the undivided and divided electrolytic cells as a function of the mixing rate (0.1 M Na_2SO_4, air purging, pH 3, 0.3 mA/cm^2, 17.9 μM Fe^{2+}, 60 min reaction)

HUJI

Abstract

The main objective of this project was to design a new electrochemical membrane cell for both monitoring and removal of micropollutants (MPs) in reused water. The first part of the work involved the application of a CNT-based flow-through system for the detection and removal of a common micropollutant, i.e., 4-nonylphenol (4-NP). This part has been successfully completed and summarized in a manuscript. A few versions or larger flow-through electrochemical cells were designed including a version that was 3D printed. We continued working on other MPs including carbamazepine (CBZ) and perfluoroalkyl substances (PFAS). This required the development of electrochemical systems for the efficient generation of ·OH radicals. We have studied the oxygen reduction reaction (ORR) using various carbon-based electrodes, such as carbon felt, carbon sponge, and CNTs. The faradaic efficiency of the formation of H_2O_2 and that of ·OH was determined. Different catalysts were examined and attached to the electrode surface. This resulted also in another manuscript. We found that the faradaic efficiency of the reduction of H2O2 using

CNTs on which a porphyrin catalyst was adsorbed was relatively very high, whereas the ORR resulted in low efficiency in the formation of ·OH radicals.

Methodology

HUJI was involved mostly in four tasks. **<u>Task 1</u>** comprised the construction of a flow-through electrochemical membrane, NEM, based on activated AC and CNTs in different configurations and adapting the state-of-the-art membrane filtration cell to electrochemical operation.

The heart of the flow-through system is the water flowing through the membrane under applied potential or current. This requires that, on one hand, high fluxes will be able to flow under moderate pressure and, on the other hand, the residence time (i.e., the time that the water is subject to the electrochemical potential) will be sufficiently high and that the diffusion layer will enable contact of the solutes with the electrode within this residence time. We took advantage of the high surface area, adsorption capacity, high conductivity, and nanometric structure of the CNTs.

Initially, we worked on a mini-scale, which means a surface area <4 cm^2 (Figure 7). As the counter electrode, we will use a stainless steel grid or a conductive Si ring. A three-electrode system, where the reference electrode (Ag/AgCl wire) was installed downstream. The potential window of the membranes was characterized and their stability was inspected by microscopy. Furthermore, analyzing the composition of the inlet and outlet water after flowing copious water was carried out.

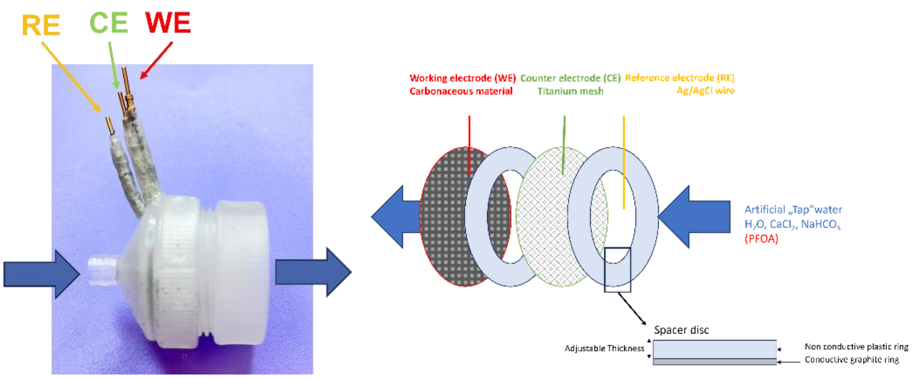

Figure 7: The electrochemical flow-through cell (left) and its scheme (right).

<u>Task 2</u> involved the investigation of the removal processes of organic micropollutants by the NanoElectroMembrane (NEM). The research examined the decomposition of

the target compounds using a direct oxidation approach as well as the electro-Fenton approach or the accumulation of them while flowing through the NEM. The removal of the compounds was determined either electrochemically or by HPLC. We studied the effect of the applied potential, flow rate, concentration and type of electrochemical membrane on the removal efficiency.

Task 3 focused on developing electrochemical protocols for monitoring the micropollutants by the NEM. We have already shown that flow-through electrochemical cells based on CNTs can be used for the very sensitive detection of metals and organic species. Similar approaches were applied here. More specifically, we studied the adsorption of a few model compounds, such as nonylphenol and its electrochemical oxidation on CNTs. The various parameters affecting the sensitivity and selectivity of the detection were studied and optimized. Finally, we were also involved in Task 7, which aimed at upscaling the NEM system to a demonstration stage (electrode surface <40 cm^2).

Results

The electrochemical detection and removal of the micropollutant 4-nonylphenol (4-NP) As a model system we chose 4-NP as a micropollutant. To successfully develop an electrochemical approach for the detection of 4-NP in recycled water, it is necessary to meet the EU or EPA regulations, which means to enable the detection of 1 ppb of 4-NP, i.e., 4.54×10^{-9} M. Figure 8 shows the CV of 10^{-6} M 4-NP using a GCE carried out in a static three-electrode cell (Figure 1A) and a CNT based flow-through cell (Figure 1B). While a very small oxidation wave can be seen with the GCE, a clear irreversible oxidation peak is observed at 0.6 V with the flow-through cell. The peak is associated with the oxidation of 4-NP and is in agreement with previous studies.

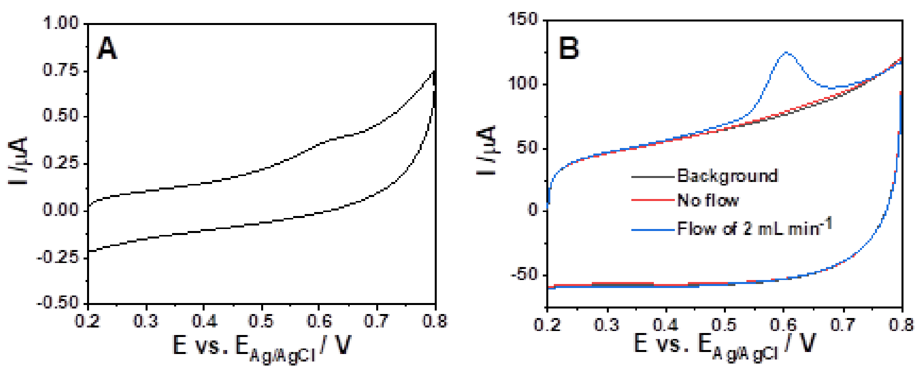

Figure 8– CV in a 10^{-6} M 4-NP and 0.1 M PBS pH 7.0 using: A) a GCE in a static cell; B) A CNT-based membrane in a flow-through cell: only buffer (black), 10-6 M 4-NP with

no flow (red) and the same concentration of 4-NP but with 2 mL min^{-1}. The scan rate was 0.1 V s^{-1}.

Next, we examined the performance of the CNT-based membrane under flow. Figure 9 shows the oxidation peak current measured after a volume of a 0.45 mM 4-NP (and 0.1 M PBS pH 7.0) solution flowed through the CNT membrane. The areal mass of the CT-50 CNTs was 0.12 mg cm^{-2}. It can be seen that a linear dependence is obtained between the volume of solution that passed through the membrane and the peak current, which implies that the adsorption sites for 4-NP on the CNT membrane were not saturated even after flowing 8 mL of 0.45 mM 4-NP.

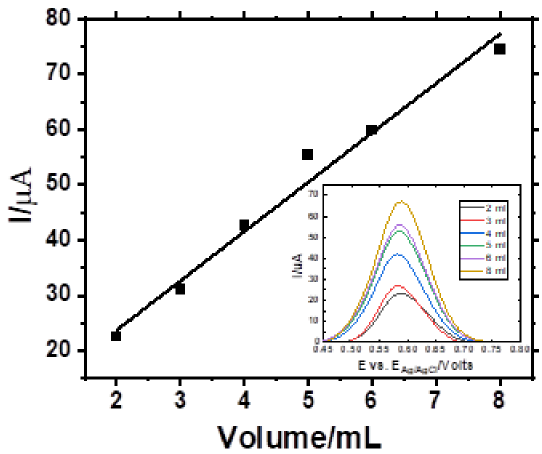

Figure 9: The oxidation peak current of 4-NP recorded with a CT-50 CNT-based membrane (0.12 mg cm^{-2}) as a function of a volume of 0.45 mM 4-NP (0.1 M PBS pH 7.0) solution flowed through the cell.

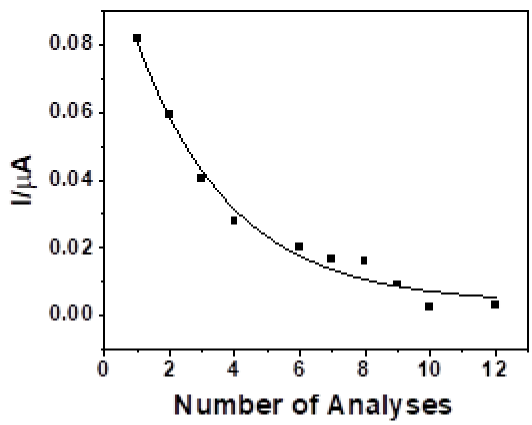

Figure 10: LSV oxidation peak currents recorded in a 4.5x10^{-7} M 4-NP and 0.1 M PBS (pH 7.0) solution as a function of the number of measurements. 4 mL of solution flowed at a rate of 2 mL min^{-1} through the flow-through cell before each measurement was performed.

Figure 10 shows the decrease in the oxidation peak current (measured by LSV) of 4.5x10^{-7} M 4-NP (0.1 M PBS pH 7.0) upon repeating the measurements without replacing the CNT electrode. 4 mL of the solution flowed (2 mL min^{-1}) through the cell before each measurement was carried out. As previously reported, the electrochemical oxidation of phenols, and 4-nonylphenol as well, creates a polymeric film that fouls the electrode surface. The latter is not fully blocked; however, it becomes less sensitive to the 4-NP and obviously cannot be used for analytical purposes.

Figure 11 shows SEM images of the CNT membrane before and after carrying multiple analyses of 1 ⍰M of 4-NP. Fouling of the CNT membrane by a carbonaceous material is evident, which is also expressed by the need to increase the pressure of the pump to keep the flow rate constant.

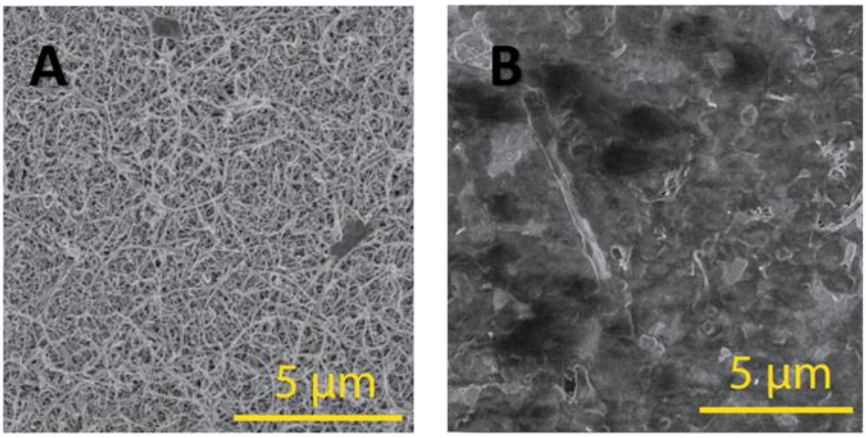

Figure 11: SEM images of the CNT membrane: A – before and B – after repeated analysis of 1 μM of 4-NP in 0.1 M PBS pH 7.0 using the flow-through cell.

Since it is not practical to replace the CNT membrane after every analysis, we carried out a set of experiments in which we applied a pulse of 10 s to the electrode with different potentials after every analysis. Figure 12 shows the LSV of 4-NP recorded after 1 mL of 4.5×10^{-7} M and 0.1 M PBS pH 7.0 flowed through the cell using the same CNT membrane. After the LSV and before another volume of solution flowed through the cell, the cleaning process of a potential pulse was applied. The red line in Figure 5A shows the signal of 4-NP obtained on a clean and new CNT membrane. It can be seen that the application of −0.6 V did not fully recover the electrode and the anodic peak current kept decreasing after each analysis. Hence, we applied a more negative pulse of −1 V (Figure 5B), which prevented the oxidation peak to further decrease, yet, the current did not fully recover its initial value. A pulse of −2 V (Figure 5C) on the other hand, caused the peak current to almost attain its initial value even after 12 consecutive analyses. This cleaning process did not add any complications and enabled us to repeatedly use the same CNT membrane.

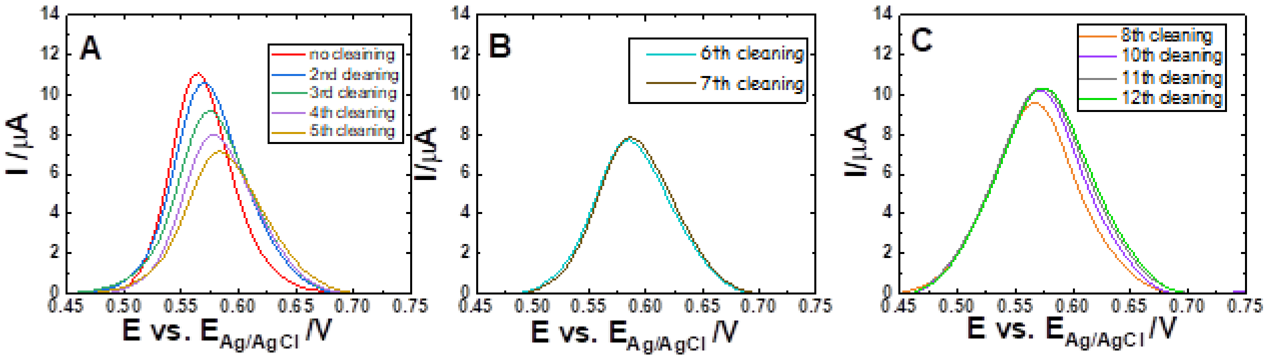

Figure 12: Cleaning the CNT membrane by a short potential pulse. Repeated LSVs of a CNT membrane, which was pulsed for 10 s at different potentials before flowing 1 mL of $4.5x10^{-7}$ M 4-NP and 0.1 M PBS pH 7.0 solution. A – −0.6 V; B – −1 V; C – −2 V.

This led us to form a calibration curve that is shown in Figure 13. The solutions with known concentrations of 4-NP flowed through the cell with a rate of 2 mL min^{-1} and LSV (0.5 V s^{-1}) was carried out after 2 mL of solution passed the CNT membrane (0.12 mg cm^{-2}). The 50 Hz noise of the grid was removed, which yielded very high sensitivity. The curve could be even further extended to 10^{-10} M, spanning three orders of concentration magnitude; however, the slope changed. The LOD for the system is $1.92 \cdot 10^{-10}$ M (equals 42.3 ppt) of 4-NP after 50 Hz filtration. This is well below the EU or EPA regulations and therefore, with some adaptation, this approach could be used for monitoring the levels of this micropollutant.

The next step was to combine electrochemical treatment and monitoring with the same flow-through electrochemical cell. Namely, as the water flows through the CNT membrane, applying a constant potential is likely to oxidize and remove the 4-NP, and the levels of the micropollutant could be determined in the same cell either with the same electrode or more likely with an additional working electrode. Therefore, we initially flowed the CNT membrane with a solution of $4.5x10^{-5}$ M 4-NP while applying different constant potentials. The outlet stream was collected and analyzed electrochemically using a GCE. Table 1 shows the removal percentage of the 4-NP.

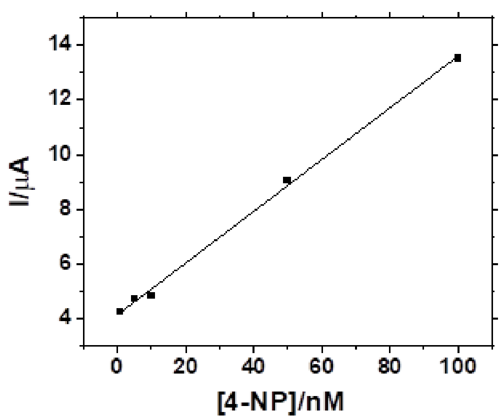

Figure 13: Calibration curve 4-NP in 0.1 M phosphate buffer, pH 7. The scan rate was 0.5 V s^{-1}.

Table 1: the removal percent of 4-NP (initial concentration was 45 mM) by applying different constant potentials and a rate of 2 mL min^{-1}.

Applied potential	Outlet [4-NP]/μM	Removal %
0.3	8.67	81
0.6	1.5	97
0.7	2.87	94
1.0	0.02	99

It can be seen that as the potential applied reaches the oxidation potential of 4-NP a significant decrease is detected in the concentration of the micropollutant in the outlet effluent. A potential of 1.0 V removes almost all the 4-NP, which suggests that the residence time of the micropollutant in the CNT membrane is sufficient for all molecules to be within electron transfer distance from the CNT.

This paved the way for the last step, i.e., removal and monitoring. To accomplish this challenge we 3-D printed a flow-through cell (Figure 14) where another CNT-membrane was added and used upstream for the detection of the levels of 4-NP in the effluent after the electrochemical treatment.

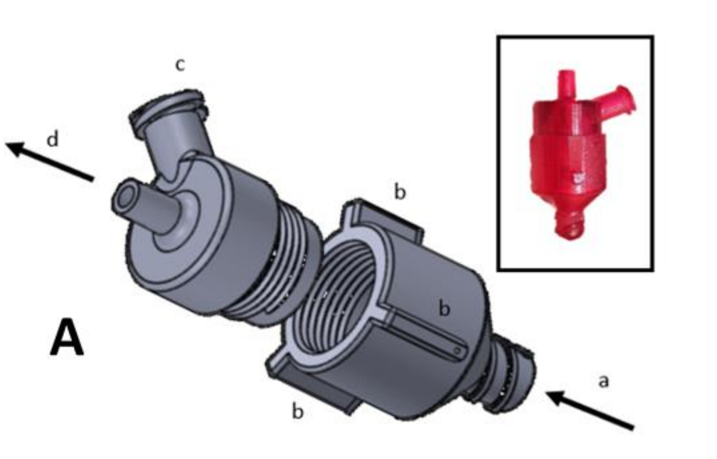

Figure 14: A – Schematics of the 3-D printed flow-through electrochemical cell; B – schematics of the cross-section of the cell.

Electrochemical generation of reactive oxygen species (ROS) on a flow-through membrane. Our approach has involved the electro-Fenton (EF) reaction that is based on the oxygen reduction reaction (ORR) to generate H_2O_2. The latter is further reduced to form $^{\cdot}OH$ radicals (eq. 1-2).

(eq. 1) $$O_2 + 2e^- + 2H^+ \rightarrow H_2O_2$$

(eq. 2) $$H_2O_2 + e^- \xrightarrow{\text{Catalyst}} {}^{\cdot}OH + OH^-$$

We started by searching for catalysts for our flow system. As can be seen in Figure 15, the ORR is evident, and the response depends both on the carbonaceous material as well as on the adsorption of different catalysts.

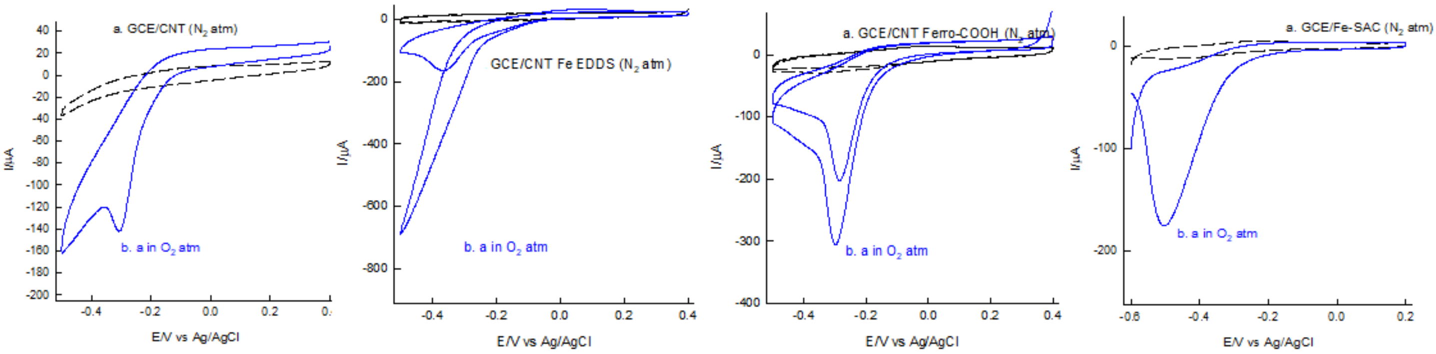

Figure 15: Cyclic voltammetry in the absence (black curves) and presence (blue curves) of oxygen using: A – glassy carbon electrode (GCE) coated with carbon nanotubes (CNT); B – CGE/CNT with Fe-EDDS; C – Ferrocene and D – Fe single-atom catalyst.

Yet, while the faradaic efficiency of the formation of H_2O_2 can be very high, that of the $^{\cdot}OH$ formation is usually below 1% (Figure 16) and most efforts are directed towards the development of efficient catalysts.

Among the catalysts that we have been using are inorganic complexes such as CoTPP (cobalt(II) tetraphenylporphyrin) and single-atom catalysts (SACs) that are attached to a carbonaceous electrode surface. Our group has started a collaboration with the Department for Chemistry at Bar-Ilan University. This group synthesizes carbon-supported SACs for the electro-Fenton reaction. The group at

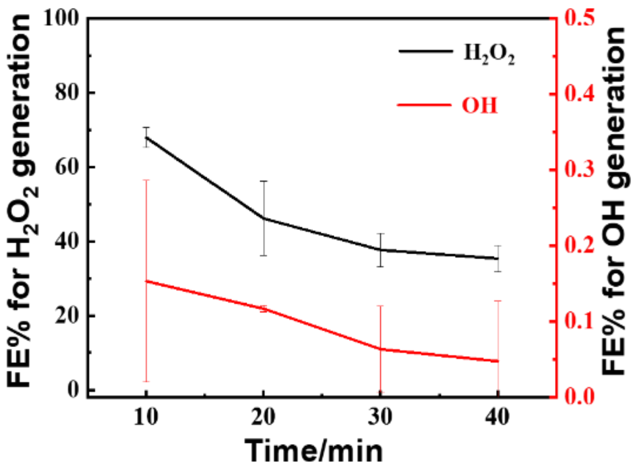

Figure 16: The faradaic efficiency of the formation of H_2O_2 and $^{\cdot}OH$ as a function of time on a carbonaceous electrode.

the Hebrew University is responsible for measuring the ability of these catalysts to improve the production of hydroxyl radicals and introduce the catalyst to the flow system.

Our initial experiments were conducted in a static cell and then we switched to a flow system, which was recently modified. The flow system can be used as a dual detection and removal device. Yet, we observed that the removal of the 4-NP that is achieved by electrochemical oxidation results in fouling of the membrane. Therefore a new system whereby two membrane electrodes are used; one for the removal and the other for the detection has been assembled by 3D printing. Figure 17 shows the faradaic efficiencies of hydrogen peroxide and hydroxyl radical formation as a function of time using different catalysts, which were synthesized at Ben Gurion University by Menny Shalom's group.

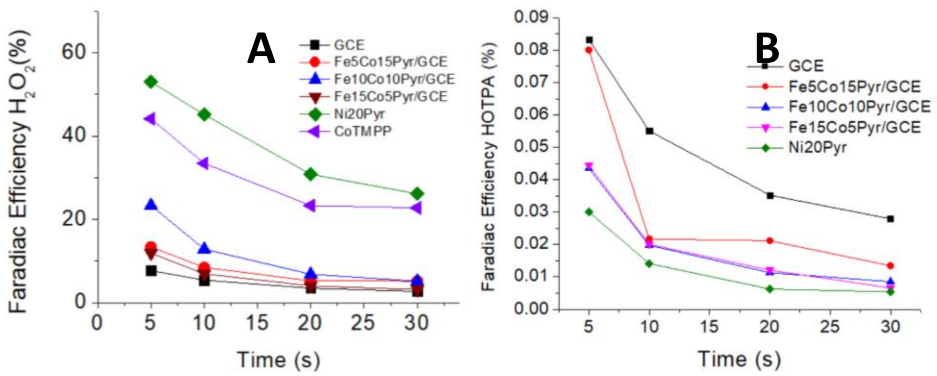

Figure 17: The faradaic efficiency of: A – H_2O_2 and B – $^{\cdot}OH$ radicals as a function of time using different catalysts.

Again, it can be seen that we still have not achieved good efficiency for the radical formation. Therefore, we are currently studying the reduction of H_2O_2 in the absence of oxygen (eq. 3).

(eq. 3) $$H_2O_2 + e^- \xrightarrow{\text{Catalyst}} {}^{\cdot}OH + OH^-$$

Figure 18 shows that indeed $^{\cdot}OH$ is formed with a faradaic efficiency of ca. 1%. This is too low and we are working now trying to improve it. It should be noted that this is still without a catalyst, yet, and based on the results above, we might need to modify the current catalysts that we are using.

One of the parameters that we are planning to change is the type of the CNTs that we apply. At present, we use MWCNTs and it seems that ORR performs much better on SWCNTs. The type of CNTs affects also the ability to form stand-alone membranes, which we make by filtering a dispersion of CNTs through a PVDF filter. MWCNTs are very difficult to separate from the support.

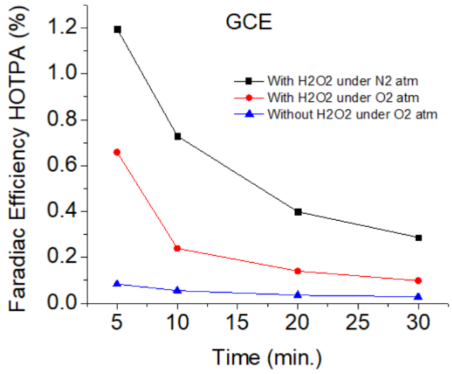

Figure 18: The faradaic efficiency of $^{\cdot}OH$ formation by the electrochemical reduction of H_2O_2

As mentioned above, we also employ inorganic complexes, such as CoTPP (Figure 5A), which is easily adsorbed on a carbonaceous material (Figure 19B). Figure 6 shows the faradaic efficiency of H_2O_2 and OH formation before and after adding the CoTPP. It can be seen that both efficiencies have increased as a result of introducing the cobalt complex.

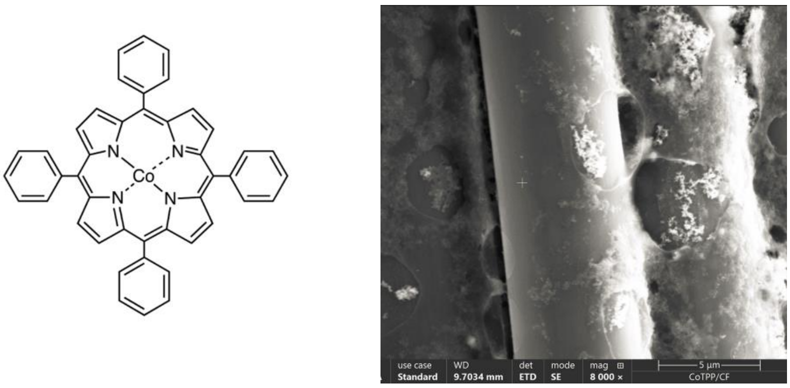

Figure 19: A – The structure of CoTPP, B – SEM image of CoTPP adsorbed on a carbon fabric used as an electrode in a flow

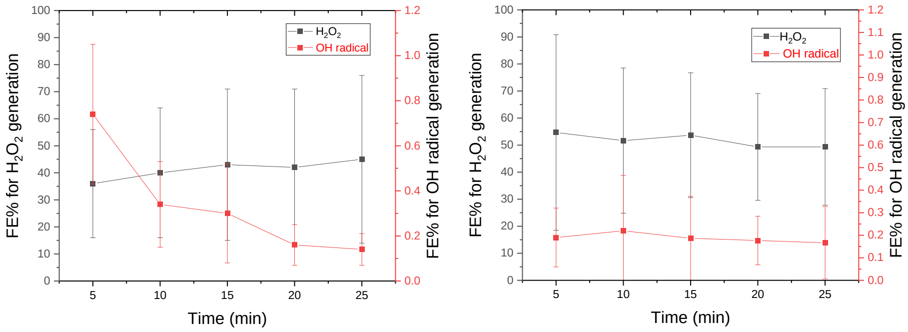

Figure 20: Faradaic efficiency of H_2O_2 and ˙OH generation before (A) and after (B) adding CoTPP to a carbonaceous electrode.

To summarize, in spite of the difficulties during the project, i.e., COVID-19 and at the end the events in Israel, we have made substantial progress. We are still summarizing some of the results in a few manuscripts but we are already looking forward to the next step in our collaboration with KIT.

KIT

Abstract

The main objectives of the German subproject include i) The design and construction of a micro-electrochemical flow-through cell, featuring a membrane area of 2 cm^2. This setup is intended for a comparative analysis with photocatalytic processes in steroid hormone (SH) micropollutant removal, highlighting advantages in throughput and cost-effectiveness. ii) Investigation of the electrochemical degradation dynamics of SH micropollutants under various operational conditions, employing a carbon nanotube (CNTs) ultrafiltration membrane supplied by David Jassby at UCLA, US. and iii) Examination of the underlying mechanisms governing both electrochemical and photocatalytic degradation of SH micropollutants. iv) The scale-up of the electrochemical filtration system from 2 to 20 cm^2, followed by an evaluation of its efficacy in SH micropollutant removal.

Methodology

1) Establishment of the micro-electrochemical flow-through system

A custom-designed micro-electrochemical flow-through cell, featuring a 2 cm^2 membrane area, was developed and its construction outsourced. This innovation aims to facilitate the study of electrochemical degradation dynamics and enable a comparative analysis with photocatalytic membrane processes for micropollutant removal, focusing on smaller scale operations for enhanced throughput and reduced experimental costs. Figure 21 presents the schematic diagram of the electro-filtration reactor.

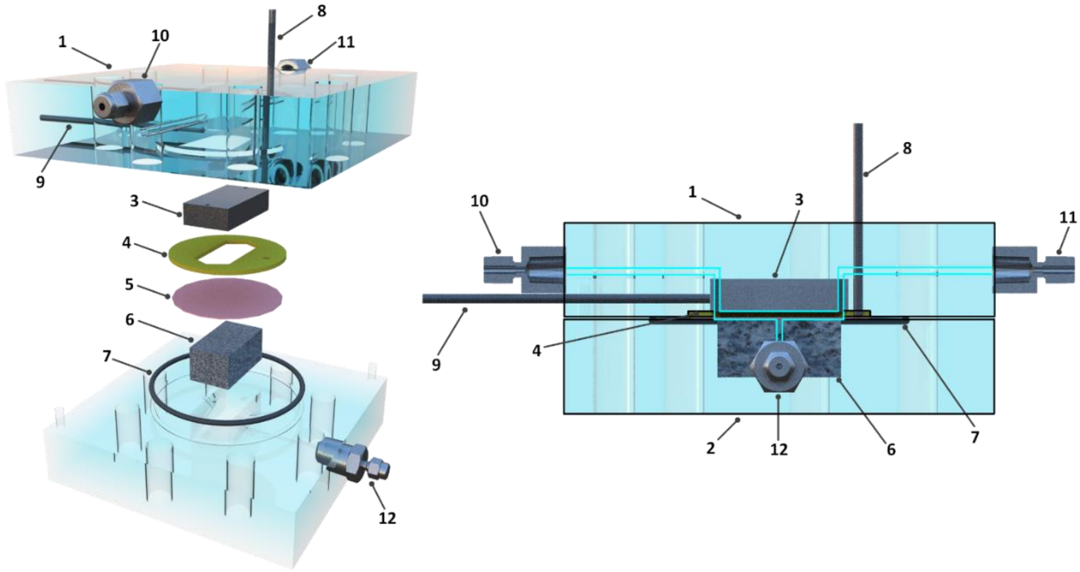

Figure 21. Schematic diagram of (Left) the exploded view, and (Right) side view of the electrochemical membrane reactor with a membrane area of 2 cm^2, 1 top cell, 2 bottom cell, 3 titanium cathode, 4 PEEK spacer, 5 electrochemical membrane, 6 titanium porous support, 7 O-ring, 8 platinum wire, 9 titanium wire, 10 feed inlet connector, 11 crossflow outlet connector, and 12 permeate outlet connector. Reprinted from [4].

The construction of the electrochemical filtration cell utilized acrylic material, incorporating a titanium sheet as the counter electrode to provide an effective electrochemical surface area of 2 cm^2. In assembling the electrochemical membrane, which functions as the anode, it was positioned above a porous support made from titanium particles (180-230 mesh). The membrane was compressed against a 0.8 mm thick polyether-ether-ketone (PEEK) spacer, strategically placed between the electrochemical membrane and the titanium cathode, to create a precisely sealed area of 2 cm^2. Platinum and titanium wires were integrated into the cell, serving as contact points for the electrochemical membrane anode and the titanium cathode, respectively.

The operating principle is to pressure water through the electro-filtration cell that contains a cathode, and an electro-membrane as anode with a constant flow rate of feed solution using a peristaltic pump. An electric field will be applied for the system to control the cell voltage between the anode and cathode when performing the electro-filtration to remove SH micropollutants.

2) Scale-up of the electrochemical filtration system from 2 to 20 cm^2

A scaled-up electro-filtration system was designed and constructed, aiming to evaluate the performance of a variety of flat sheet electro-membranes, including ultra- and micro-filtration (UF and MF) electro-membranes, in SH micropollutants removal during water reuse processes with an extended membrane area. Configuration and flow diagram of the designed electro-filtration system are presented in Figure 22.

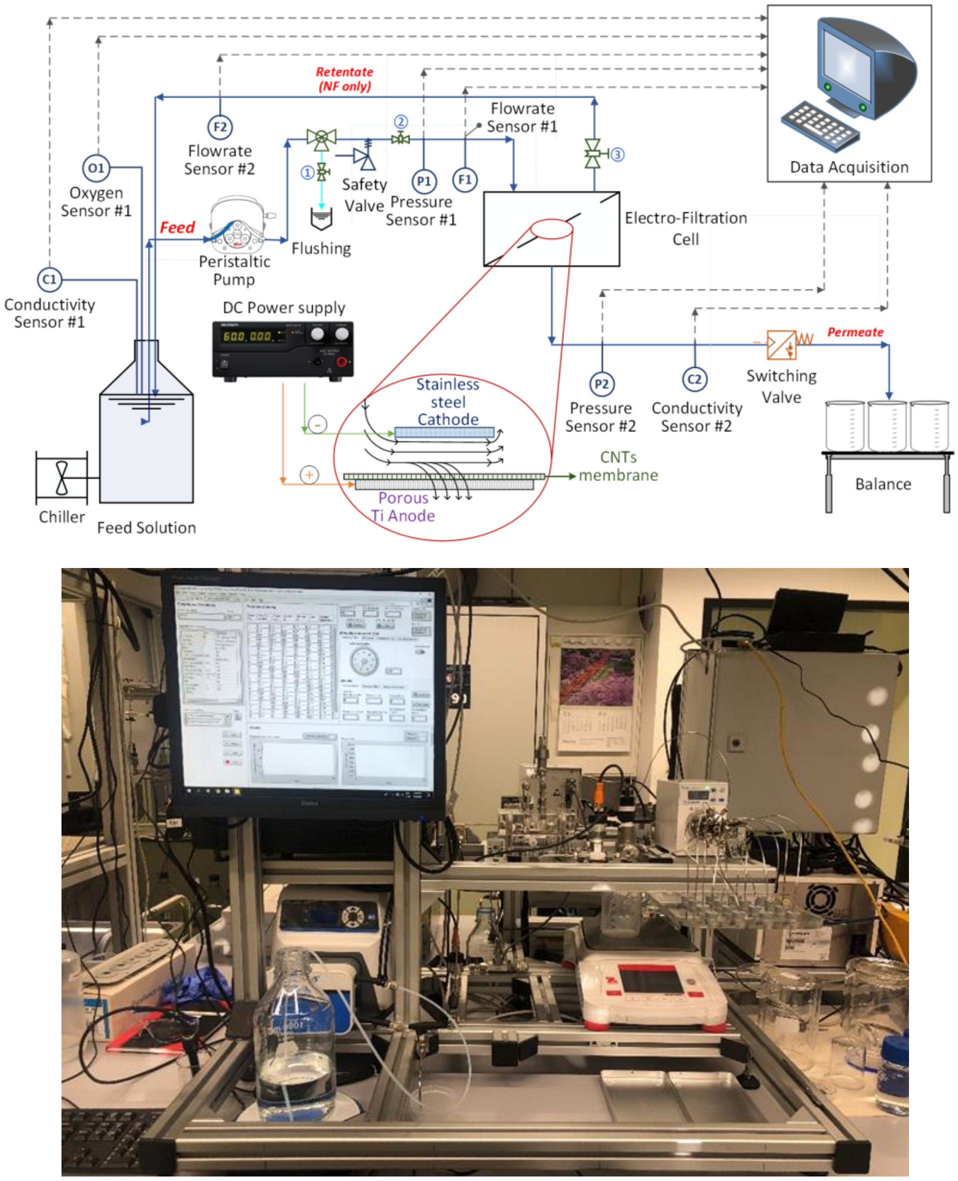

Figure 22. Schematic and picture of the established electro-filtration system. Reprinted from [4].

Central to this system is a commercial electrochemical filtration cell (Figure 23, model CF016A, SterliTech, USA [5]). This cell is designed to accommodate an electrochemical membrane as a flow-through anode, and a stainless steel plate as a cathode, providing an effective filtration area of 20 cm^2. Other key components of the setup include: a direct current power supply to regulate the voltage across the electrochemical cell, and a peristaltic pump that allows flow rate ranging from 0 to 92 mL/min, a 16-port switching valve, which facilitates the automatic collection of permeate samples, a balance is employed to measure the mass of the permeate, and a data acquisition card is used to acquire and transfer data from the various sensors and the balance to a computer for analysis. The operation of the peristaltic pump, power supply, and switching valve is integrated and automated through a LabView program interface (version 20.0.1, National Instruments, USA).

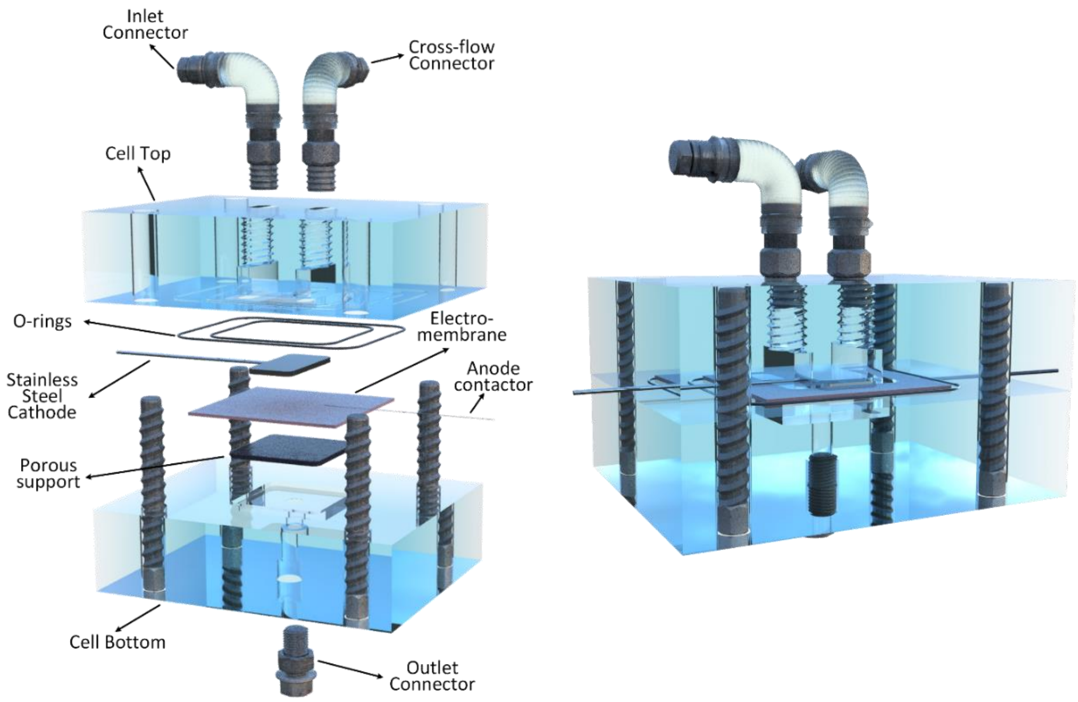

Figure 23. Schematic diagram of the electrochemical membrane reactor with membrane area of 20 cm^2. Reprinted from [6].

<u>3) Development of analytical method for differentiation between electrochemical adsorption and degradation of SH micropollutant</u>

An innovative methodological approach was developed, integrating a Liquid Scintillation Counter (LSC) and an Ultra High-Performance Liquid Chromatograph (UHPLC) coupled with a Flow Scintillator Analyzer (FSA), to unravel the mechanisms of SH removal by the EMR, focusing specifically on the simultaneous processes of degradation and adsorption. The UHPLC-FSA method, adapted from Lyubimenko et al. [1], is deployed for high-resolution separation of sample constituents. This enables precise identification and quantification of both the intact SH compound and its degradation byproducts that may form within the system. Such separation is essential for a comprehensive understanding of the chemical behavior of SH during electrochemical reactions. In parallel, the LSC technique quantifies the total ^3H activity within the samples, providing an exhaustive assessment of all radiolabelled species present, whether they are the parent compound or its degradation products.

This synergistic application of advanced analytical techniques provides an in-depth insight into the complex chemical and physical reactions occurring within the electrochemical matrix, enhancing our understanding of the underlying mechanisms of the electro-filtraiton system.

Results

1) Degradation performance of the electrochemical membrane reactor for steroid hormone micropollutant

The electrochemical degradation of micropollutant with a carbon nanotube (CNTs) ultrafiltration membrane (provided by David Jassby at UCLA, US [2]) was examined at a cell voltage of 1.6 V and a flux of 600 L/m^{2}h (Figure 24), which demonstrated a remarkable removal over 98% (limited currently by analytical detection limit). This performance is particularly notable when compared to the photocatalytic membrane process utilizing a PES-TiO_2 membrane under UV irradiation, which reported a removal of 47±8% under the same flux and a significantly higher energy consumption (10 mW/cm^2) [7].

As illustrated in the chromatograms (Figure 24D), alongside the reduction in E2 concentration, three distinct byproducts were identified based on their unique retention times—approximately at 3, 5, and 8 minutes—utilizing UHPLC-FSA. The normalized ^3H concentration in the permeate was found to be in alignment with the combined concentrations of intact E2 and its three transformation products, as quantified by UHPLC-FSA, according to mass balance analysis. This evidence suggests that these three byproducts are the primary intermediates of E2 degradation within the CNT EMR (Figure 24C).

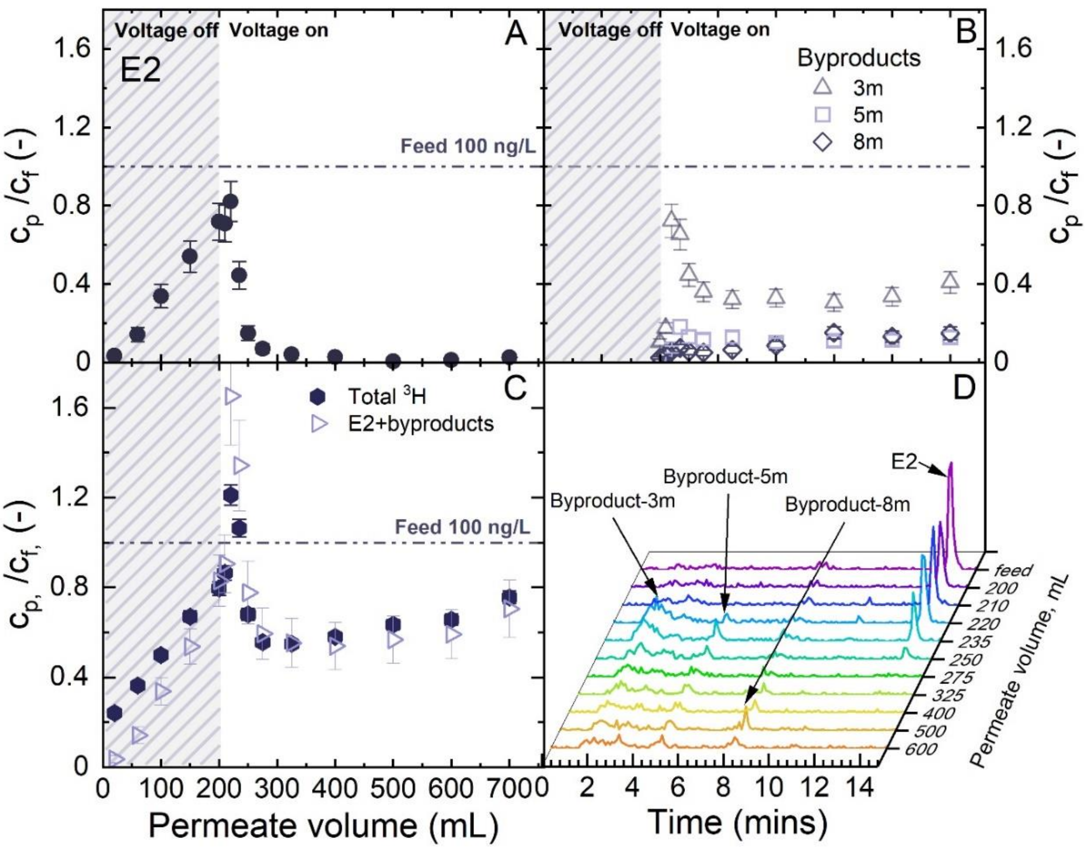

Figure 24. Electrochemical degradation of E2 within CNT EMR as normalized concentration of (A) E2 ($c_{p,E2}/c_{f,E2}$), (B) byproducts ($c_{p,met}/c_{f,met}$), (C) 3H, and the sum of E2 and the three byproducts vs. accumulated permeate volume, and (D) UHPLC-FSA chromatograms of E2 during the electrochemical degradation with increasing accumulated permeate volume. $c_{f,E2}$ = 100 ng/L, V_{cell} = 1.6 V, J_f = 600 L/m^{2}h (2 mL/min), 1 mM $NaHCO_3$, 10 mM NaCl, 27.2 mg/L EtOH, 79.2 mg/L MeOH, pH 8.2±0.2, 23±0.2 °C. Reprinted from [4]

2) Limiting factors determined in the electrochemical membrane reactor

The limiting factors of the EMR were systematically identified across a range of operational conditions (cell voltage, flux, concentration), thereby providing deep insights into the mechanisms of EMR in the treatment of micropollutants.

Applied cell voltage determines the rate of electron transfer rate at the membrane surface. To delve deeper into the extent to which the rate of electron transfer could limit the electrochemical degradation of E2, experiments were conducted across a spectrum of cell voltages, ranging from 0.9 to 3 V (Figure 25).

When cell voltages of 0.9 V and 1.05 V were applied, the CNT EMR demonstrated relatively modest E2 removal of 13±10% and 22±8%, respectively (Figure 25A). A slight increase in voltage to 1.2 V—surpassing the critical potential required to initiate E2 electrooxidation, markedly improved E2 removal to 94±2%. Furthermore, at voltages exceeding 1.2 V, E2 removal efficiency reached 99±1%, with the removal rate stabilizing at a plateau of approximately 5±0.3 mol/m²s. This plateau indicates a regime limited by surface concentration.

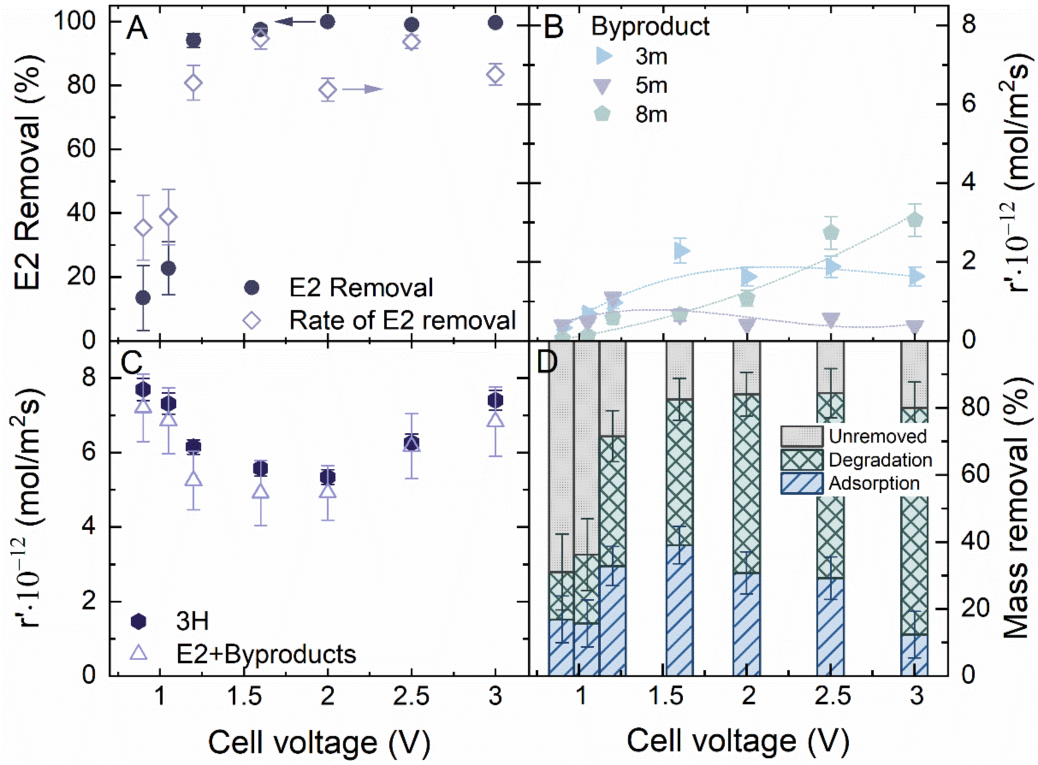

Figure 25. Impact of cell voltage on the electrochemical degradation of E2 expressed as (A) E2 removal and apparent rate of E2 removal, and (B) apparent rate of byproduct formation, (C) 3H, and the sum of E2 and the three byproducts in permeate; and (D) contribution to the mass removal of E2 by the electrochemical adsorption and degradation vs. cell voltage. $c_{f,E2}$ = 100 ng/L, J_f = 600 L/m²h (2 mL/min), 1 mM $NaHCO_3$, 10 mM NaCl, 27.2 mg/L EtOH, 79.2 mg/L MeOH, pH 8.2±0.2, 23±0.2 °C. Reprinted from [4]

The hydraulic residence time (t_r) of micropollutants within the EMR is regulated by the water flux, which plays a crucial role in shaping the interaction dynamics between the micropollutants and the membrane. An extended hydraulic residence time enhances the likelihood of micropollutant molecules encountering and adsorbing onto the electron transfer sites on the membrane surface. To ascertain the flux threshold necessary to enter the hydraulic-residence-time-independent regime within the CNT-based EMR, a sequence of experiments was performed with water flux ranging from 60 to 3000 L/m²h (Figure 26). Correspondingly, the t_r was observed to decrease from $40\cdot10^{-3}$ to $0.8\cdot10^{-3}$ s within this range.

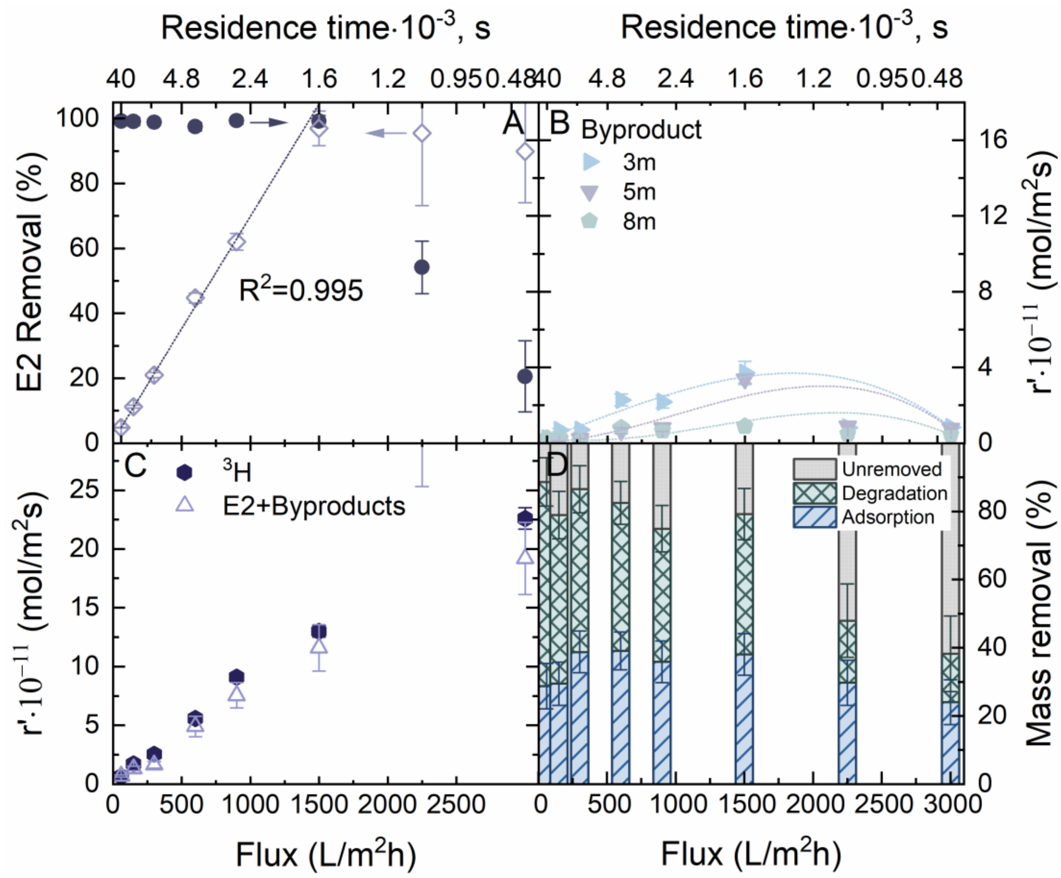

Figure 26. Impact of water flux on the electrochemical degradation of E2 expressed as (A) E2 removal and apparent rate of E2 removal, and (B) apparent rate of byproduct formation, (C) 3H, and the sum of E2 and the three byproducts in permeate; and (D) contribution to the mass removal of E2 by the electrochemical adsorption and degradation vs. flux. $c_{f,E2}$ = 100 ng/L, V_{cell} = 1.6 V, 1 mM $NaHCO_3$, 10 mM NaCl, 27.2 mg/L EtOH, 79.2 mg/L MeOH, pH 8.2±0.2, 23±0.2 °C. Reprinted from [4].

A robust linear correlation (R^2=0.995) was found between the shortening hydraulic residence time, from $39.6 \cdot 10^{-3}$ to $1.6 \cdot 10^{-3}$ s (corresponding to an increase in flux from 60 to 1500 L/m²h), and the rate of E2 removal. As the flux increased, the rate of E2 removal rose linearly from $(0.6 \pm 0.02) \cdot 10^{11}$ to $(12 \pm 0.6) \cdot 10^{11}$. This suggests that at hydraulic residence times less than $1.6 \cdot 10^{-3}$ s, the kinetics of the electrochemical reaction were constrained by the availability of E2 molecules within the EMR per unit time. Upon further increasing the flux to 3000 L/m²h, the rate of E2 removal reached a plateau, indicating a shift to an electron-transfer-limited regime. In this regime, the rate of the electrochemical reaction is insufficient to regenerate the CNT membrane surface for additional adsorption. The pronounced transition from mass-limited to electron-transfer-limited regimes can be attributed to the direct electron transfer mechanism's strong reliance on the availability of electrochemical sites.

To explore the possibility that the degradation kinetics of E2 within the EMR are influenced by its initial concentration, electrochemical filtration experiments were conducted across a range of E2 concentrations, from 50 to 10^6 ng/L (Figure 27).

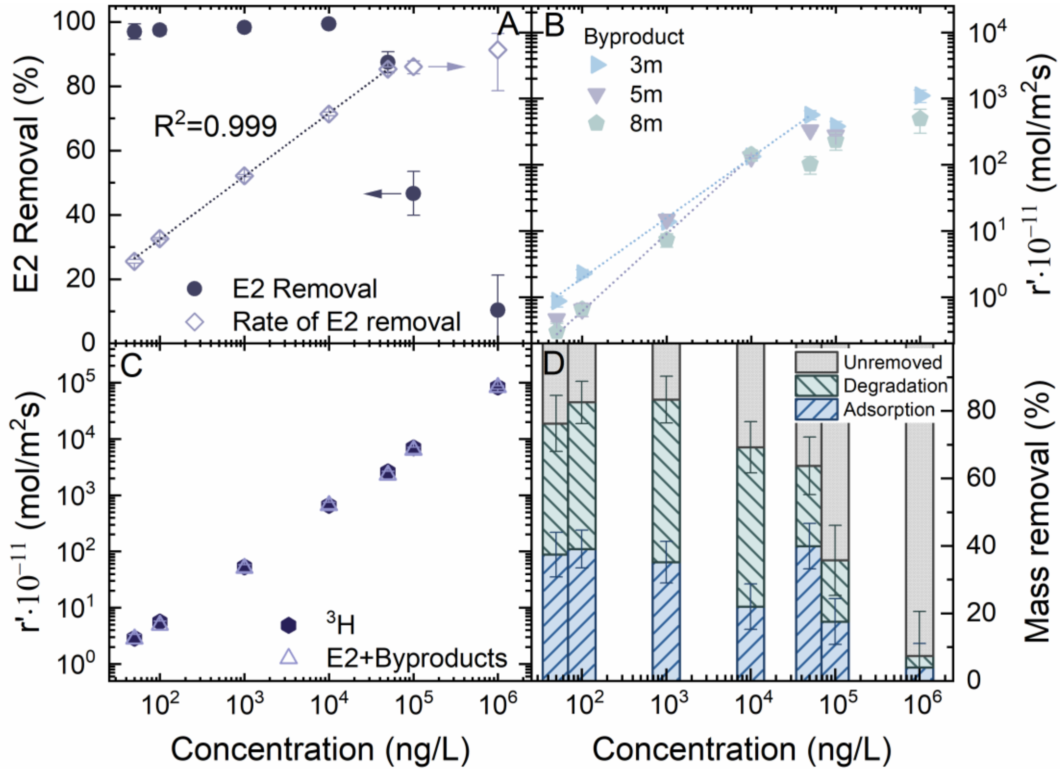

Figure 27. Impact of initial concentration on the electrochemical degradation of E2 expressed as (A) E2 removal and apparent rate of E2 removal, and (B) apparent rate of byproduct formation, (C) 3H, and the sum of E2 and the three byproducts in permeate; and (D) contribution to the mass removal of E2 by the electrochemical adsorption and degradation vs. temperature. $c_{f,E2}$ = 100 ng/L, V_{cell} = 1.6 V, J_f = 600 L/m2h (2 mL/min), 1 mM NaHCO3, 10 mM NaCl, 27.2 mg/L EtOH, 79.2 mg/L MeOH, pH 8.2±0.2. 23±0.2 °C. Reprinted from [4].

Figure 27A reveals a clear linear relationship (R^2 = 0.999) between the apparent rate of E2 removal and its initial concentration, covering a range from 50 to $5{\cdot}10^4$ ng/L, before reaching a plateau at concentrations above $5{\cdot}10^4$ ng/L. This behavior suggests a reaction regime that is limited by the availability of E2 molecules at the membrane surface for concentrations between 50 and $5{\cdot}10^4$ ng/L. Remarkably, the removal rate plateaus at a maximum of $(3.8 \pm 2.9){\cdot}10^{-9}$ mol/m^{2}s once the E2 concentration exceeds $5{\cdot}10^4$ ng/L. This pronounced change signifies a shift from a concentration-limited regime to one dictated by surface area availability, indicating that the reactive sites on the membrane interface become saturated with adsorbed E2 molecules.

<u>3) Degradation mechanisms (heterogeneous *vs.* homogeneous) within the electrochemical and photocatalytic membrane processes</u>

To elucidate the degradation mechanisms of SH within the CNT EMR, the principal reactive species involved, notably hydroxyl radicals (·OH [8, 9]) and active chlorine ([10, 11]), were identified across a range of cell voltages from 0.9 to 3V (Figure 28).

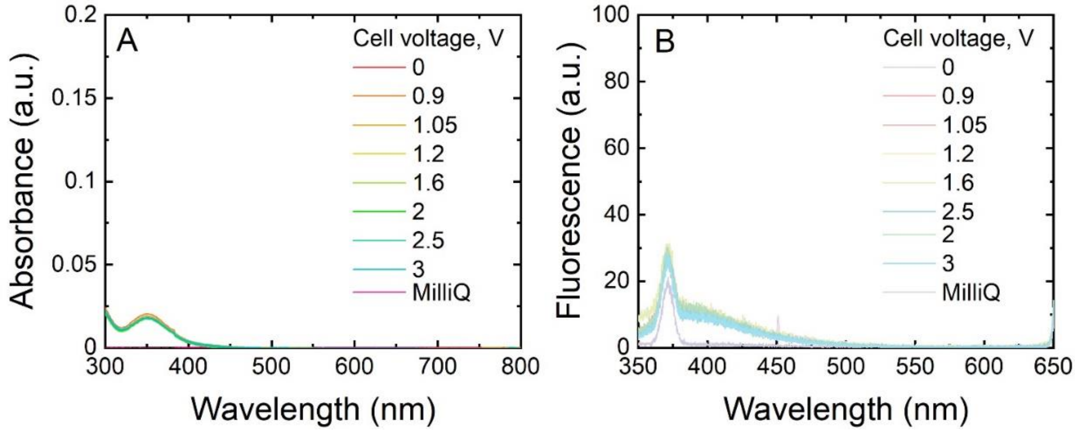

Figure 28. (A) Absorbance spectra of active chlorine in the permeate sample for filtration of a KI/NaAc/HAc solution at varying cell voltage from 0.9 to 3 V within the CNT EMR, and (B) fluorescence spectra of ·OH adduct in permeate for electrochemical filtration with 200 mL of coumarin solution at varying cell voltage from 0.9 to 3 V within the CNT EMR. $c_f(coumarin)$ = 0.01 mM, J_f = 600 L/m2h (2 mL/min), 10 mM NaCl, 1 mM NaHCO3, 27.2 mg/L EtOH, 79.2 mg/L MeOH, pH 8.3±0.3, 23±0.2 ℃. Reprinted from [4].

Figure 28A reveals that the absorbance at 352 nm for the permeate sample, across a range of applied voltages, matches that of the blank sample. This suggests that no measurable active chlorine was produced in the EMR, even under voltages as high as 20 V. The fluorescence spectra (Figure 28B) exhibited two features associated with water scattering and coumarin, yet no peaks corresponding to ·OH-coumarin byproducts were detected. This indicates that no significant ·OH radicals were generated by the CNT membrane under the tested conditions. These findings lead to the inference that direct electron transfer plays a central role in the degradation of SH, supported by fundamental electrochemical studies on the CNT membrane, which included cyclic voltammetry (CV) measurements (Figure 29).

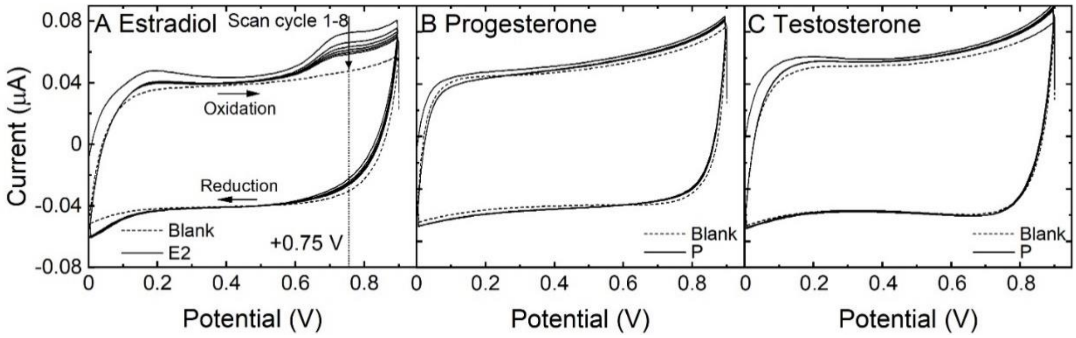

Figure 29. Cyclic voltammograms for 1 mg/L (A) estradiol, (B) progesterone, and (C) testosterone in electrolyte containing 10 mM NaCl, 1 mM $NaHCO_3$, 27.2 mg/L EtOH, and 79.2 mg/L MeOH in potentential range from 0 to 0.9 V with a scan rate of 100 mV/s. Reprinted from [4].

An anodic oxidation peak for E2 was identified at a potential of +0.75 V (*vs.* Ag/AgCl), with no discernible reduction peak in the reverse scan (Figure 29A). This observation points to the irreversible electrooxidation of E2 through direct electron transfer on the CNT membrane. Direct electron transfer is postulated to engage E2 in the liberation of two protons, leading to the formation of a phenoxy radical. This radical is capable of resonance within the aromatic ring, eventually transforming into a ketone derivative [12-14]. Such a chemical modification significantly alters the estrogenic activity of E2, primarily through changes to its phenolic binding group [15, 16]. The continued oxidation of E2 is anticipated to yield lower molecular weight compounds, potentially culminating in its complete mineralization to CO2.

To confirm the hypothesis of electron transfer mechanism in the E2 degradation within the CNT EMR, $NaNO_3$ was employed as a scavenger to target surface electrons (Figure 30).

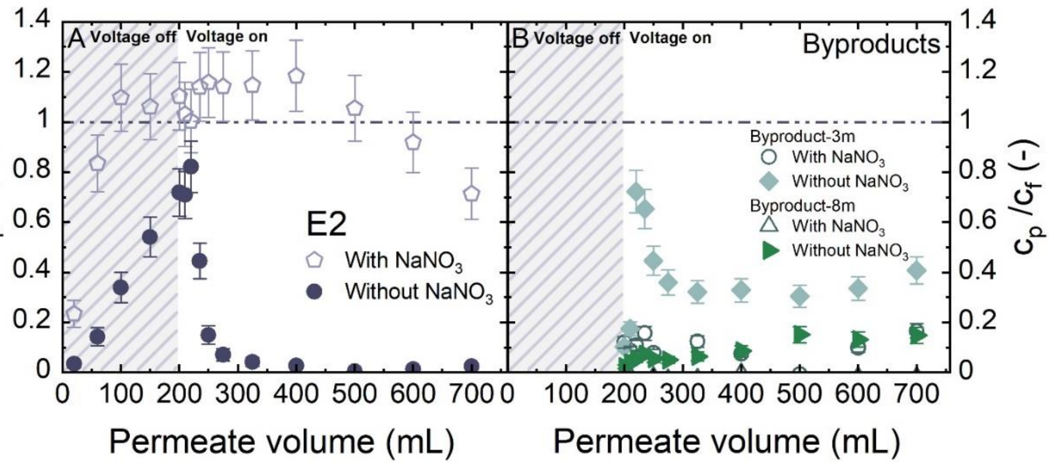

Figure 30. Electrochemical degradation of E2 in the presence of scavenger NaNO3 for surface electrons within the CNT EMR, as normalized concentration of (A) E2 and,

and (B) byproducts, vs. accumulated permeate volume. $c_{f,E2}$ = 100 ng/L, $c_{f,NaNO_3}$ = 10 mM, V_{cell} = 1.6 V, J_f = 600 L/m^{2}h (2 mL/min), 1 mM $NaHCO_3$, 10 mM NaCl, 27.2 mg/L EtOH, 79.2 mg/L MeOH, pH 8.2±0.2, 23±0.2 °C. Reprinted from [4].

The addition of 10 mM $NaNO_3$ notably hindered the removal of E2 in the CNT EMR, resulting in only minimal production of the degradation byproduct-3m. This outcome suggests that direct electron transfer is the dominant mechanism driving E2 degradation in the EMR.

To determine the contribution of different reactive species to the photocatalytic degradation of E2, the experiments were conducted with 1 and 10 mM of various scavengers (Figure 31).

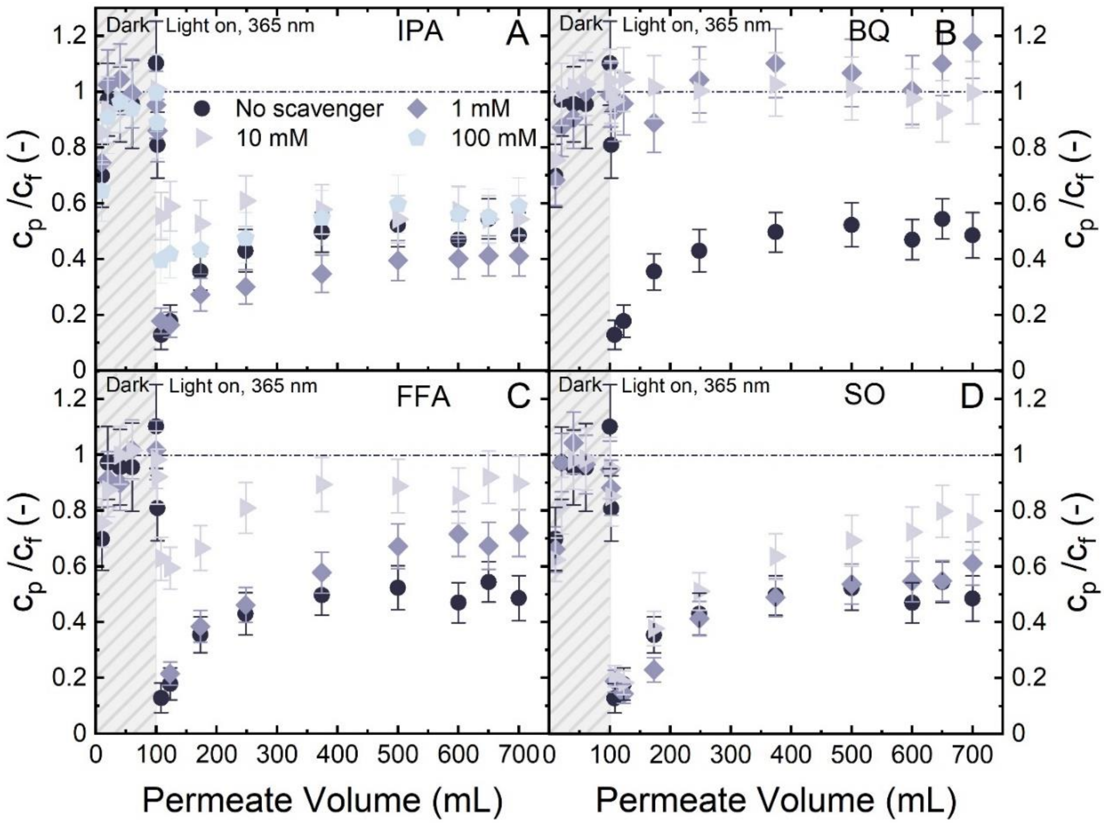

Figure 31. Effect of 1 and 10 mM (A) IPA, (B) BQ, (C) FFA, and (D) SO on the photocatalytic degradation of E2 (0.003 mM) expressed as normalized permeate concentration of E2 ($c_{p,E2}/c_{f,E2}$) vs. cumulative permeate volume (V_p). PES-TiO2, $c_f(E2)$ = 100 ng/L, I_{inc} = 10 mW/cm2, 365 nm, J_f= 600 L/m2h, 1 mM NaHCO3, 10 mM NaCl, 27.2 mg/L EtOH (0.3 mM), 79.2 mg/L MeOH (2.5 mM), pH 8.3±0.3, 23±0.2 °C. Data adapted from [17].

The presence of either 1 or 10 mM IPA did not significantly impact the degradation of E2 in the PMR system, suggesting that ·OH did not play a role in the degradation process. This lack of effect may be attributed to the scavenging action of the buffer solution components—ethanol, methanol, and $NaHCO_3$—on the ·OH radicals. Conversely, the introduction of either 1 or 10 mM BQ completely halted E2 removal. BQ is known to react with both $\cdot O_2^-$ and ·OH, but given that IPA, a known ·OH scavenger, did not influence E2 degradation, it's logical to deduce that $\cdot O_2^-$ is the primary ROS responsible for E2 removal in the PMR system.

The E2 removal dropped from 47±8% to 26±8% and 7±9% with the addition of 1 and 10 mM FFA, respectively. FFA can interact with both $^1O_2$ and ·OH. However, the reduction in E2 removal, despite the presence of FFA, underscores that while $^1O_2$ may contribute to E2 degradation, its role is significantly less critical compared to $\cdot O_2^-$. An alternative explanation could be that FFA scavenges a minor fraction of $\cdot O_2^-$ [18], thus diminishing E2 removal efficiency. No discernible impact was observed with SO, which suggests that valence band holes (h_{VB}^+) either do not contribute or contribute minimally to E2 degradation.

Reference

[1] R. Lyubimenko, B.S. Richards, A. Turshatov, A.I. Schäfer, Separation and degradation detection of nanogram-per-litre concentrations of radiolabelled steroid hormones using combined liquid chromatography and flow scintillation analysis, Scientific Reports, 10 (2020) 7095

[2] X. Zhu, A.V. Dudchenko, C.M. Khor, X. He, G.Z. Ramon, D. Jassby, Field-induced redistribution of surfactants at the oil/water interface reduces membrane fouling on electrically conducting carbon nanotube UF membranes, Environmental Science & Technology, 52 (2018) 11591-11600

[3] D. Jassby, M. Wiesner, C.-f. De Lannnoy, Electrically conducting reverse osmosis membranes, in, U.S. Patent 9,802,163, Issued October 31, 2017.

[4] D.J. Siqi Liu, Andrea I. Schäfer, Removal of steroid hormone in a carbon nanotube electrochemical membrane reactor: Adsorption, degradation, and formation of metabolites, (2024)

[5] CF016A electrode modified crossflow assembly, acrylic, in, https://www.sterlitech.com/cf016a-electrode-modified-crossflow-assembly-acrylic.html.

[6] S.L.D.J.D.M.A.I. Schäfer, Removal of steroid hormone micropollutants by electrochemical carbon nanotubes membrane in a flow-through reactor: Differentiation between electrochemical adsorption and degradation, (2024)

[7] S. Lotfi, K. Fischer, A. Schulze, A.I. Schäfer, Photocatalytic degradation of steroid hormone micropollutants by TiO_2-coated polyethersulfone membranes in a continuous flow-through process, Nature Nanotechnology, 17 (2022) 417-423

[8] K. Jiang, S. Back, A.J. Akey, C. Xia, Y. Hu, W. Liang, D. Schaak, E. Stavitski, J.K. Nørskov, S. Siahrostami, H. Wang, Highly selective oxygen reduction to hydrogen

peroxide on transition metal single atom coordination, Nature Communications, 10 (2019) 3997
[9] H. Liu, C.D. Vecitis, Reactive transport mechanism for organic oxidation during electrochemical filtration: Mass-transfer, physical adsorption, and electron-transfer, Journal of Physical Chemistry C, 116 (2012) 374-383
[10] W.-L. Wang, Q.-Y. Wu, N. Huang, T. Wang, H.-Y. Hu, Synergistic effect between UV and chlorine (UV/chlorine) on the degradation of carbamazepine: Influence factors and radical species, Water Research, 98 (2016) 190-198
[11] E. Brillas, I. Sirés, Electrochemical remediation technologies for waters contaminated by pharmaceutical residues, in: E. Lichtfouse, J. Schwarzbauer, D. Robert (Eds.) Environmental Chemistry for a Sustainable World: Volume 2: Remediation of Air and Water Pollution, Springer Netherlands, Dordrecht, 2012, pp. 297-346.
[12] M.M. Ngundi, O.A. Sadik, T. Yamaguchi, S.-i. Suye, First comparative reaction mechanisms of β-estradiol and selected environmental hormones in a redox environment, Electrochemistry Communications, 5 (2003) 61-67
[13] Y. Ohko, K.-i. Iuchi, C. Niwa, T. Tatsuma, T. Nakashima, T. Iguchi, Y. Kubota, A. Fujishima, 17β-estradiol degradation by TiO_2 photocatalysis as a means of reducing estrogenic activity, Environmental Science & Technology, 36 (2002) 4175-4181
[14] J. Mai, W. Sun, L. Xiong, Y. Liu, J. Ni, Titanium dioxide mediated photocatalytic degradation of 17β-estradiol in aqueous solution, Chemosphere, 73 (2008) 600-606
[15] Y. Zhao, J. Hu, W. Jin, Transformation of oxidation products and reduction of estrogenic activity of 17β-estradiol by a heterogeneous photo-Fenton reaction, Environmental Science & Technology, 42 (2008) 5277-5284
[16] A.M. Brzozowski, A.C.W. Pike, Z. Dauter, R.E. Hubbard, T. Bonn, O. Engström, L. Öhman, G.L. Greene, J.-Å. Gustafsson, M. Carlquist, Molecular basis of agonism and antagonism in the oestrogen receptor, Nature, 389 (1997) 753-758
[17] S. Liu, P.C. Edara, A.I. Schäfer, Influence of organic matter on the photocatalytic degradation of steroid hormones by TiO_2-coated polyethersulfone microfiltration membrane, Water Research, 245 (2023) 120438
[18] Y. Guo, J. Long, J. Huang, G. Yu, Y. Wang, Can the commonly used quenching method really evaluate the role of reactive oxygen species in pollutant abatement during catalytic ozonation?, Water Res, 215 (2022) 118275

2. CONCLUSIONS

Despite the difficulties in the pandemic, the Israeli and German group have collaborated closely and finalized most of the proposed tasks of the project. This project integrated nanotechnologies with electrochemical reactions in a composite membrane to achieve in-situ monitoring of micropollutants (MPs) in polluted or reused (treated) water, and remove micropollutants effectively in water reuse. The main outcomes of includes:

i) The efficiency of homogeneous and heterogeneous Fenton-like oxidation processes in removing propoxur (PR) was investigated in a submerged ceramic membrane reactor operated in a continuous mode. A freshly prepared amorphous heterogeneous catalyst was synthesized and characterized, revealing a layered porous structure of 5–16 nm nanoparticles that formed aggregates (33–49 µm) known as ferrihydrite (Fh). The membrane exhibited a rejection of >99.6% for Fh. The homogeneous catalysis (Fe^{3+}) exhibited better catalytic activity than the Fh in terms of PR removal efficiencies.

ii) A novel electrochemical membrane cell was developed for both monitoring and removing MPs, including 4-NP, CBZ, and PFAS, from reused water. Several configurations of larger flow-through electrochemical cells were created, including a 3D-printed version. The faradaic efficiencies for the formation of H_2O_2 and ·OH were assessed using various carbon-based electrodes, such as carbon felt, carbon sponge, and CNTs. The results indicated that the faradaic efficiency for H_2O_2 reduction was exceptionally high when CNTs coated with a porphyrin catalyst were used, although the oxygen reduction reaction (ORR) displayed low efficiency in generating ·OH radicals.

iii) The electrochemical degradation of SHs using an ultrafiltration membrane immobilized with CNTs in a single-pass flow-through EMR was investigated at environmentally realistic concentrations (50 – 10^6 ng/L). The CNT EMR demonstrated high efficiency in eliminating E2 from a feed solution of 100 ng/L, utilizing a cell voltage of 1.6 V and a water flux of 600 $L/m^2h\cdot bar$ (flow rate 2 mL/min), which achieved a permeate concentration below the detection limit (2.5 ng/L) after treatment. Direct electron transfer was identified as the primary mechanism driving the degradation of SHs in the CNT EMR, whereas superoxide radicals was found to dominate the mechanisms of MP degradation in a photocatalytic membrane.

These results highlight the significant potential of integrating nanotechnologies into electrochemical membrane processes for monitoring MPs and reusing water. Building on these achievements, the Israeli group from HUJI and the German group from the KIT have submitted a joint proposal for funding through the BMBF-MOST program to scale up the application of this electrochemical membrane process for agricultural wastewater reuse.

3. PUBLICATIONS, PATENTS, INVENTIONS:

- Abed-Alhakeem Azaiza, Raphael Semiat, Hilla Shemer. Competitive Study of Homogeneous and Heterogeneous Fenton-like Flow-through Propoxur Oxidation in ROC Solution. Water Science & Technology 87(11), 2023, 2890–2904.
- Siqi Liu, Pattabhiramayya C. Edara, Andrea I. Schäfer*. Influence of organic matter on the photocatalytic degradation of steroid hormones by TiO_2-coated polyethersulfone microfiltration membrane. Water Research, (2023) 245: 120438.
- Siqi Liu, Eléonore Véron, Shabnam Lotfi, Kristina Fischer, Agnes Schulze, Andrea I. Schäfer*. Poly(vinylidene fluoride) membrane with immobilized TiO_2 for degradation of steroid hormone micropollutants in a photocatalytic membrane reactor. Journal of Hazardous Materials, (2023) 447:130832.
- Siqi Liu, David Jassby, Daniel Mandler, Andrea I. Schäfer*. Removal of steroid hormone micropollutants by electrochemical carbon nanotubes membrane in a flow-through reactor: Differentiation between electrochemical adsorption and degradation. (2024) Submitted.
- Siqi Liu, David Jassby, Andrea I. Schäfer* Removal of steroid hormone in a carbon nanotube electrochemical membrane reactor: Adsorption, degradation, and formation of metabolites. (2024) In preparation.